Hydrothermal assisted morphology designed MoS_2 material as alternative cathode catalyst for PEM electrolyser application

S. M. Senthil Kumar[*, A], *K. Selvakumar* [A], *R. Thangamuthu* [A], *A. Selvi* [B], *S. Ravichandran* [B], *G. Sozhan* [B], *K. Rajasekar* [C], *Nuria Navascues*[D], *Silvia Irusta* [D]

[A] Electrochemical Materials Science Division, CSIR-Central Electrochemical Research Institute, Karaikudi-630006, Tamil Nadu, India.

[B] Electro Inorganic Chemical Division, CSIR-Central Electrochumical Research Institute, Karaikudi 630003, Tamil Nadu, India

[C]Department of Nanotechnology, Anna University, Regional Centre, Coimbatore-641047, Tamil Nadu, India.

[D] Department of Chemical and Environmental Engineering, Aragon Nanoscience Institute 50018-Zaragoza, Spain

In this work, we developed a simple and cost-effective hydrothermal route to regulate the formation of molybdenum disulfide (MoS_2) in different morphologies, like, nano-sheet, nano-hollow-sphere and nano-flake structure by controlling the reaction temperature and sulphur precursor employed. Such a fine tuning of different morphologies yields a leverage to obtain novel shapes with high surface area to employ them as suitable candidates for hydrogen evolution catalysts. Moreover, we report here the first time observation of MoS_2 nano-hollow-sphere formation via hydrothermal route and characterized them by X-ray diffraction (XRD), nitrogen adsorption and desorption by Brunaer–Emmett-Teller (BET) method, scanning electron microscopy (SEM), transmission electron microscopy (TEM), High-angle annular dark-field scanning transmission electron microscopy (HAADF-STEM) and X-ray photo-electron spectroscopy (XPS) techniques. MoS_2 nano-spheres exhibits superior activity towards hydrogen evolution reaction (HER) with a low over-potential 120

mV (RHE), accompanied by large exchange current density and excellent stability in 0.5 M H_2SO_4 solution.

Key words: MoS_2, nano-shapes, electro-catalyst, hydrogen evolution reaction, exchange current density, Tafel plot

Corresponding Author E-mail: smsk_2k@ yahoo.com, senthilkumarsm@ cecri.res.in

Introduction

Search towards efficient, cost-effective catalysts for the large scale production of hydrogen gas is under immense scrutiny for the realisation of hydrogen based economy. The existing catalysts of Pt group metals for the hydrogen evolution reaction (HER) are highly efficient [1] but too expensive and their scarcity on earth make them not viable for mass production. In this contest, replacing the expensive and rare catalysts with earth-abundant materials attracts scientific curiosity toward making the hydrogen production more economic and competitive [2]. In the recent past, many potential alternate catalysts have been developed for HER which includes metal sulphides [3-7], selenides [8,9], borides [10], carbides [10,11], nitrides [12-14]. Among all these alternatives, molybdenum disulfide (MoS_2) has received significant attention due to the earth-abundant composition and high activity, leading to the development of various kinds of MoS_2-based HER electrocatalysts in the form of the crystalline [15-22] or amorphous nature [23-25].

MoS_2 belongs to a large family of two dimensional (2D) layered metal chalcogenide materials. Similar to the graphene layers in graphite, individual sandwiched S-Mo-S layers are held together by weak vander Walls interactions in hexagonally packed structures. Both experimental [18] and computational [26] studies have concluded that the catalytic activity arises from active sites located along the edges of 2D MoS_2 layers, while the basal surface are catalytically inert. It is well known that the unsaturated sulphur atoms on the edges play a crucial role in HER catalysis. Hence increasing the number of unsaturated sulphur atoms is

an efficient pathway to enhance the HER activity. Besides the aspect of active sites, the electric conductivity of catalyst is another crucial factor to affect the electro-catalytic activity because a high conductivity ensures a fast electron transport during the catalytic process [27-30].

The rational design and construction of materials with structure-sensitive properties at the nanoscale is extremely important in developing advanced nanomaterials. Novel properties may arise when the size of a material is decreased to nanoscale and the dimensionality is lowered, due to quantum confinement effect and edge effects [31,32]. Although MoS_2 has been proved an exciting hydrogen evolution reaction (HER) catalyst but its activity is limited by constrains in exposure of active edge sites, poor electrical transport and inefficient electrical contact. As a result, tremendous efforts have been made to design and engineer the structure of MoS_2 catalysts with exposed active sites. Moreover, the morphology and distribution of the catalytically important edge sites of MoS_2 are found to be sensitive to preparation conditions. In this work we highlighted a scalable pathway to accomplish the task of engineering MoS_2 nano-shape which in turn manifests to expose more active sites. We achieved this by designing a reaction with suitable Mo precursor along with sulphur source during hydrothermal process in order to realize controllable morphology with more active sites. We have employed both TEM and HAADF-STEM microscopic technique to uncover the facts behind methodology tuned nanoscale morphology. Moreover the resultant MoS_2 materials have been employed as electro-catalysts toward HER in 0.5 M sulphuric acid and by using linear sweep voltammetry (LSV) technique to demonstrate the structure-activity relationship.

2. Experimental Section

Sodium molybdate (Na_2MoO_4; 98% purity) from Sigma Aldrich, Thioaceteamide (CH_3CSNH_2; 98% purity) from Merck, Thiourea (H_2N-CS-NH_2; 99% purity) from Sigma Aldrich, Nafion from Sigma Aldrich, Hydrochloric Acid, Ethanol were analytical grade and used without further purification.

2.1 Materials Preparation

Sodium molybdate (Na_2MoO_4; 98%) 10 m.mol and Thioaceteamide (CH_3CSNH_2; 98%) 30 m.mol were dissolved in 50 mL of deionized water. Then, 10 mol/L HCl was dropped into the solution and stirred well to adjust the pH value to 1. After ultrasonic dispersion for about 30 min, the solution was transferred into a 100 ml Teflon-lined stainless steel autoclave and heated at a temperature 200 °C (named as S01), 240 °C (named as S02) individually for 36 hours. After cooling to room temperature, the resulting precipitates were collected by filtration, rinsed with copious amounts of deionized water and further heat-treated at 400 °C for 2 h in a Quartz tubular furnace with flowing argon gas atmosphere (99.99%). Both the heating and cooling rate were set as 5 $^oC\ min^{-1}$.

In another process, 0.05 mol of sodium molybdate (Na_2MoO_4; 98%) was added into 40 mL deionized water and stirred until it dissolved completely. Next, 0.15 mol thiourea (H_2N-CS-NH_2; 99%) was added into the above mixture and a milky white suspension was obtained after 2 hours of vigorous stirring. Then, the suspension was transferred into a 100 mL Teflon-lined autoclave and the temperature was maintained at 240 °C for 36 h (named as S03). The final product was rinsed three times with deionized water and ethanol, after that the sample was dried at 60 °C for 10 h.

2.2 Characterisation of MoS_2 materials

The crystalline nature of the different MoS_2 materials were examined by powder X-ray diffraction (XRD) measurements using a PAN Analytical X′ Per PRO Model X-ray

Diffractometer with Cu K_α radiation (λ = 1.5418 Å) from 10º to 80º at 0.02º step and a count time of 0.2 s. N_2 sorption isotherm for determining BET surface area and BJH pore size distribution was measured (Quantachrome Instruments NOVA 4000e) at 77 K. The X-ray photoelectron analysis (XPS) was performed with an Axis Ultra DLD (Kratos Tech.). The spectra were excited by the monochromatized AlKα source (1486.6 e.V) run at 15 kV and 10 mA. For the individual peak regions, a pass energy of 20 eV was used. Survey spectrum was measured at 160 eV pass energy. Analyses of the peaks were performed with the CasaXPS software, using a weighted sum of Lorentzian and Gaussian components curves after background subtraction. The binding energies were referenced to the internal C 1s (284.9 eV) standard. The field-emission scanning electron microscopy (FE-SEM) was performed on a Carl Zeiss AG Supra 55VP with an acceleration voltage of 5–30 kV. Nanostructure morphology and compositional studies were performed by conventional transmission electron microscopy (TEM), in a FEI Tecnai T20 operated at 200 kV. High-angle annular dark-field scanning transmission electron microscopy (HAADF-STEM) and corresponding energy-dispersive spectroscopy (EDS) mapping analyses was performed on a FEI Tecnai F30 operated at 300 kV with a spherical aberration corrector.

2.3 Electrochemical Measurements

Electrochemical measurements were performed in a three-electrode system at an electrochemical work station AUTOLAB potentiostat (model PGSTAT 302N). Typically, 2.37 mg of MoS_2 powder was dispersed in 0.5 mL of a solution composed of 4:1 (v/v) distilled water and ethanol containing 0.5% (w/w) Nafion by sonication for 1 h to form a homogeneous slurry. Then 3 µl of the slurry was added on the surface of glass carbon electrode with 3 mm diameter (loading ca. 0.2 mg cm^{-2}). Linear sweep voltammetry with scan rate of 2 mV s^{-1} was conducted in 0.5 M H_2SO_4 (purged with pure N_2) using saturated

calomel electrode (SCE) as the reference electrode, a graphite rod as the counter electrode. All the potentials were calibrated to a reversible hydrogen electrode (RHE).

3. Results and Discussions

3.1 Influence of reaction condition and precursor on MoS_2 formation

The synthesized electro catalysts have been characterized by X-ray diffraction in order to understand the formation of the MoS_2 material. **Figure 1** shows the XRD patterns of the three different samples prepared in this work. The figure clearly indicates that the MoS_2 prepared from sodium molybdate and thioacetamide precursor at 200 ºC (i.e., S01) displays a single peak in XRD positioned at 2θ value of 15º which corresponds to (002) plane of MoS_2 sample (JCPDS card number 37-1492) due to insufficient crystallization under this temperature. However, the MoS_2 prepared from same set of precursor but at 240 ºC posses well defined diffraction peaks at 2θ values ca. 15º, 32º, 40º and at 60º corresponds to (002), (100), (103) and (110) planes and matches well with the values of JCPDS card number 37-1492 [33]. In case of S02 sample, the occurrence of high intensity peaks including (002) when compared to S01 shows that the formation of a crystalline hexagonal form of MoS_2 with a well-stacked layered structure requires a temperature of 240 ºC during hydrothermal process. It proves the fact that temperature plays an important role in determining the crystalline nature of MoS_2 nano-material. Similarly, S03 material synthesized using different sulphur precursor ca. thiourea but with identical temperature conditions of 240 ºC produces well defined diffraction peaks at their respective 2θ values as shown in **Fig.1**. Therefore, from the above observations it can be understood that the formation of MoS_2 from sodium molybdate and thioacetamide or with thiourea precursor requires a temperature of 240 ºC.

3.2 Morphological differences of MoS_2 materials

Figure 2 shows the FE-SEM images of the three different MoS_2 materials prepared in this work. It is clear that each sample possess its own intrinsic morphology, for example the S01 catalyst shows a thin sheet like morphology where as the S02 material posses sphere like structure with 10 to 100 nm diameter. Moreover, it can be clearly seen that few of the damaged sphere walls indicates that spheres are made up of hollow inner space. Such type of MoS_2 material with a morphology composed of nano-hollow-sphere has not been reported earlier to the best of our knowledge. Unlike S02, the S03 catalyst displayed a single MoS_2 flake with few hundred nm in length. It is demonstrated that even though all the three catalysts prepared through hydrothermal procedure but with a slight variation in temperature and precursor type could lead significant alterations in the resultant nano-structures and morphologies.

TEM analysis were performed on the three type of catalysts prepared in this work are presented in **Fig. 3**. When the synthesis temperature is as low as 200 ºC (S01), structures of not-well developed shapes made up of obscure edges can be obtained, indicating the insufficient crystallization under this condition (**Fig 3A& B**). In contrast to this while at 240 ºC (S02) synthesis temperature with the same composition of precursors, a well developed spheres with a wall thickness of 5-10 nm were obtained as shown in **Fig 3C & D**. However, the change in sulphur source from thioacetamide to thiourea under identical experimental conditions (S03) yields curled flakes like structure as shown in **Fig 3E**. Moreover, as shown in **Fig 3F**, the calculated lattice space value of 0.29 nm from TEM is in good agreement with a value of 0.27 nm calculated from XRD and corresponds to (100) plane. The curled flake like structure may possess internal voids and cavities that could be the reason for the observed high BET surface area value of 36. 2 m^2/g when compared to 28.5 m^2/g obtained for (S02) MoS_2 sample (see support information **Fig S3** and **Table S1**). In case of both (S02) and (S03) catalysts, the observed BET surface area values are ~3 times higher than the value 10.6

m^2/g observed for a ball-milled Micro-MoS_2 in a high-energy planetary mill with stainless steel balls as milling media [34].

Furthermore, the high angle annular dark-field scanning transmission electron microscopy (HAADF-STEM) and EDS mapping analysis has been already employed on oxygen enriched layered MoS_2 very recently [35]. This method is capable of providing information regarding the elemental distribution on a given three dimensional structure and was carried out on S02 sample in order to examine whether the sphere is composed of empty space or filled with active MoS_2 material. **Figure 4A & B** represents the HAADF-STEM image and its corresponding EDS mapping depth profile from sampling spot A to B as marked in the figure. It is interesting to note the EDS mapping of Mo and S elements which proves clearly that the elements are seen abundant and enriched selectively on walls of the sphere. In contrast to this the inner volume of the sphere is left as hollow space (similar to empty egg-shell type structure) as shown in images **Fig. 4C**, **D** and **E**. It is worth to mention here that similar observation of hollow nano-structure formation of carbon materials through hydrothermal method has been reported recently by Titirici group [36]. Moreover, in our method, thioacetamide plays a role of reducing agent and sulphur donor during the whole hydrothermal process, in which thioacetamide releases H_2S as a sulphide source as well as a reducing agent, resulting in the reduction of MoO_4^{2-} precursors to MoS_2. The reaction routes for the synthesis of MoS_2 by thioacetamide could be expressed as follows [37]:

$$2\ CH_3CSNH_2 + 4\ H_2O \rightarrow 2\ CH_3COOH + 2\ NH_3 + 2\ H_2S \text{ ---(R1)}$$

$$4\ MoO_4^{2-} + 9\ H_2S + 6\ CH_3COOH \rightarrow 4\ MoS_2 + SO_4^{2-} + 6\ CH_3COO^- + 12\ H_2O \text{ ---(R2)}$$

3.3 XPS studies on MoS_2 materials

In order to investigate the chemical composition of the synthesized MoS_2 material, XPS analyses were carried out. Fig. 5 shows spectra of the Mo 3d core level for the prepared samples. Mo $3d_{5/2}$ peaks around 229.5 eV and Mo $3d_{3/2}$ peaks around 232.5 eV are the most important features in S02 and S03 spectra suggesting that the dominant oxidation state present in these samples is Mo^{4+} [16]. Only traces of Mo^{6+} are observed in S03 spectrum while in S02 spectrum peaks related to Mo^{6+} and Mo^{5+} are present . On the other hand, sample S01 shows the presence of more than 60 at. % of Mo^{6+} and up to 9 at.% of Mo^{5+} (see Table S2) clearly showing that at a hydrothermal reaction temperature of 200 ºC thioacetamide does not carry out the complete reduction of the precursor. Such circumstances leads to the formation of MoS_2 with insufficient crystallization as discussed in previous section. On the other hand in case of S02, at a reaction temperature of 240 ºC with same composition of Na_2MoO_4 and thioacetamine MoS_2 was obtained which is evidenced from the strong peaks observed at 229.1 and 232.1 eV as shown in **Fig. 5B**. However, still the presence of significant quantity of Mo^{6+} in this material (18 at.%) proves the presence of un-reduced precursors even under this condition. It is worth to note that the MoS_2 material prepared by employing thiourea precursor at 240 ºC (S03) shown only a trace amount of Mo^{6+} state in **Fig. 5C**. It proves that thiourea effectively performs the reduction process as explained in above equations R1 and R2.

Figure 6 represents the XPS typical peaks for S 2p region of MoS_2 samples studied in this work. It can be seen that the S 2p region is also influenced by the nature of the method employed for the preparation of MoS_2 materials. For the chemical state of S^{2-} in MoS_2 spectra shows a doublet with $S2p_{3/2}$ peak at 162.3 eV [Britt A. Vanchura , Pingang He , Valentyn Antochshuk , Mietek Jaroniec ,* Amy Ferryman , Dmytro Barbash , Julia E. Fulghum , and Songping D. Huang, *J. Am. Chem. Soc.*, 2002, 124 (41), pp 12090–12091]. These doublet, 162.5 and 163.7 eV for $S2p_{3/2}$ and $S2p_{1/2}$ respectively is the main feature in S03 **(Fig. 6C)**, with just traces of SO_4^{2-}

showed by the presence of a doublet at 169,9-170.1 eV [J. Baltrusaitis, C. R. Usher and V. H. Grassian, *Physical Chemistry Chemical Physics*, 2007, **9**, 3011-3024.]. Besides these two chemical environments for S, sample S02 also presents sulphur as terminal S^{2-} and/or S_2^{2-} showed by the presence of peaks at 162.9 and 163.4 eV (**Fig. 6B**) [T.-W. Lin, C.-J. Liu and J.-Y. Lin, *Applied Catalysis B: Environmental*, 2013, **134–135**, 75-82]. In sample S01 this last chemical environment became predominant as can be seen in **Fig. 6A**.

3.4 Electrochemical hydrogen evolution studies on MoS_2 catalysts

The electrochemical studies were carried out by employing linear sweep voltammetry technique at a scan rate of 2 mV s^{-1} in nitrogen saturated 0.5 M H_2SO_4 electrolyte solution. **Figure 7A** shows the comparison of LSV curves recorded for all three MoS_2 catalysts prepared in this work and also for a Pt electrode studied in the potential range from + 0.2 V to – 0.4 V (RHE). All the measurements were carried out at a constant MoS_2 loading of 0.2 mg cm^{-2}. As shown in **Fig.7A**, among the MoS_2 materials, nano-hollow-sphere (S02) catalyst posses much lower onset potential than nano-sheet (S01) and nano-flake (S03) MoS_2 catalysts. Among all, (S02) nano-hollow-sphere MoS_2 exhibits the lowest on-set value of 120 mV, suggesting the superior HER activity. Cathodic current density is considered as an important evaluating criterion for HER activity. As shown in **Fig 7B**, S02 exhibits significantly large cathodic current density with a moderate Tafel slope value when compared with other two types of MoS_2 catalysts studied in this work. Three principle steps for converting H^+ to H_2 have been proposed for HER in acidic medium on a Pt surface [38, 39]. The first is a primary discharge step (i.e., Volmer reaction, equ 1)

$$H_3O^+ + e^- \rightarrow H_{ads} + H_2O \text{ ---(1)}$$

Followed by the primary discharge step, the electrochemical desorption step (i.e., Heyrovsky reaction, equ 2) or recombination step (i.e., Tafel reaction, equ 3) may be involved

$H_{ads} + H_3O^+ + e^- \rightarrow H_2 + H_2O$ ---(2)

$H_{ads} + H_{ads} \rightarrow H_2$ ---(3)

Tafel slope is an inherent property of electrocatalysts that is determined by the rate-limiting step of HER. Under a specific set of conditions, when the Volmer reaction is the rate-limiting step of HER, a slope of 120 mV decade $^{-1}$ should be observed, whereas if Heyrovsky or Tafel reactions act as the rate-limiting step, Tafel sloes of 30 and 40 mV decade $^{-1}$ can be obtained respectively [38, 39]. For a complete HER process, combinations of steps, i.e., Volmer-Heyrovsky or Volmer-Tafel mechanism, should be involved to produce molecular hydrogen. Although the HER mechanism for MoS_2 still remains inconclusive due to the reaction complexity, the Tafel slope of 124, 102, 148 mV decade $^{-1}$ were observed for our MoS_2 catalysts S01, S02 and S03 respectively as shown in **Table 1**. These values are indeed very close to the value of 140 mV decade $^{-1}$ reported for a CVD grown single layer MoS_2 coated glassy carbon electrode for HER reported very recently [40].

A comparison of the exchange current densities (j_0), Tafel slopes and onset potentials of various molybdenum sulphide catalysts investigated in the literature reports is shown in **Table 1**. One can see that MoS_2 nano-hollow-sphere (S02) catalyst prepared in this work shows much larger exchange current density, smaller onset potential along with a moderate Tafel slope among the pure MoS_2 catalysts. It can be inferred that there are more active sites in the nano-hollow-sphere MoS_2 catalyst due to the sphere structures, which can generate a larger current at low over-potentials and make it reach the critical value at a more positive over-potential. However, higher intrinsic electric resistance between the interlayers of the MoS_2 spheres limits the electron transfer, resulting in a larger Tafel slope compared to

layered MoS_2 materials as shown in **Table 1**. It is worth to mention here that few attempts have been already pursued to overcome the poor conductivity of the material by the introduction of Au [18, 20] and carbon materials [42, 43] which attests better electrical conductivity leads improved electron transfer which in turn reducing the Tafel slope values. However, it must be noted that the MoS_x catalyst without any additions still shows a much lower Tafel slope, probably attributed to the rich S edges, but the exact definition of active sites for these amorphous structures is still not very clear [20, 24]. Besides the HER activity, stability is another significant criterion to evaluate an advanced electrocatalyst. To investigate the stability in acidic environment, long-term cycling stability of nano-hollow-sphere MoS_2 (S02) is investigated by performing continuous cyclic voltammetry (CV) between - 0.3 and 0.1 V [RHE] at 50 mV s^{-1}. A negligible difference was observed between the LSV curves measured at the initial cycle and after 1000 cycles of CV operation, suggesting the excellent durability of nano-hollow-sphere MoS_2 (S02) catalyst during long-term cycling.

Conclusions

In summary, we have synthesized an efficient MoS_2 catalyst with a controlled nano-hollow-sphere by controlled hydrothermal reaction between sodium molybdate and thioacetamide precursors at 240 ºC. The structure of the nano-hollow-sphere MoS_2 has been confirmed by FE-SEM, TEM and HAADF-STEM analysis. This specific structured MoS_2 presents excellent catalytic performance for HER. The significant enhancement of catalytic activity of nano-hollow-sphere when compared with other two shapes prepared in this work is attributed to the abundance of exposed edge sites. The improved performance of this catalyst towards HER is evidenced by the small overpotential of ~120 mV and a moderate Tafel slope when compared with other MoS_2 materials studied in this work. The construction of structure-sensitive nano-materials with enhanced HER activity provide a feasible way to

design and engineer advanced nanostructures for catalysis, solar-water splitting devices and other potential applications.

Acknowledgements

The authors appreciate the financial support from CSIR through 12th FYP project MULTIFUN (CSC 0101). We would like to thank our Director Dr. Vijayamohanan K. Pillai for his constant support and suggestions. The authors also thank the staff members of Central Instrument Facility of CSIR-CECRI for their tremendous help and valuable contributions. We also thank Prof. K. Chandrasekara Pillai for his constant support and guidance.

References

1. J. Greeley, T. F. Jaramillo, J. Bonde, I. Chorkendorff, J. K. Norskov, Nature. Mater. , 5 (**2006**) 909.
2. E. Casado-Rivera, D. J. Volpe, L. Alden, C. Lind, C. Downie, T. Vazquez-Alvarez, A. C. D. Angelo, F. J. DiSalvo, H. D. Abruna, J. Am. Chem. Soc. 126 (**2004**) 4043.
3. D. Voiry, H. Yamaguchi, J. Li, R. Silva, D. C. B.Alves, T. Fujita, M. Chen, T. Asefa, V. B. Shenoy, D. Eda, M. Chhowalla, Nature. Mater. , 12 (**2013**) 850.
4. D. Merki, S. Fierro, H. Vrubel, X. Hu, X. Chem. Sci., 2 (**2011**) 1262.
5. D. Merki, X. Hu, Energy Environ. Sci., 4 (**2011**) 3878.
6. H. Vrubel, D. Merki, X. Hu, Energy Environ. Sci., 5 (**2012**) 6136.
7. J. Kim, S. Byun, A. J. Smith, J. Yu, J. Huang, J. Phys. Chem. Lett., 4 (**2013**) 1227.
8. D. Kong, H. Wang, J. J. Cha, M. Pasta, K. J. Koski, J. Yao, Y. Cui, Y., Nano Lett., 13 (**2013**) 1341.
9. M. R. Gao, S. Y. Lin, T. T. Zhuang, J. Jiang, Y. F. Xu, Y. R. Zheng, S. H. Yu, J. Mater. Chem., 22 (**2012**) 13662.

10. H. Vrubel, X. Hu, Angew. Chem., Int. Ed., 51 (**2012**) 12703.

11. W. F. Chen, C. H. Wang, K. Sasaki, N. Marinkovic, W. Xu, J. T. Muckerman, Y. Zhu, R. R. Adzic, Energy Environ. Sci., 6 (**2013**) 943.

12. X. Hu, B. S. Brunschwig, J. C. Peters, J. Am. Chem. Soc., 129 (**2007**) 8988.

13. P. A. Jacques, V. Artero, J. Pecaut, M. Fontecave, Proc. Natl. Acad. Sci. U.S.A. 106 (**2009**) 20627.

14. E. S. Andreiadis, P. A. Jacques, P. D. Tran, A. Leyris, M. Chavarot Kerlidou, B. Jousselme, M. Matheron, J. Pecaut, S. Palacin, M. Fontecave, V. Artero, Nat. Chem., 5 (**2013**) 48.

15. J. Xie, H. Zhang, S. Li, R. Wang, X. Sun, M. Zhou, J. Zhou, X. W. Lou, Y. Xie, Adv. Mater., 25 (**2013**) 5807.

16. J. Kibsgaard, Z. Chen, B. N. Reinecke, T. F. Jaramillo, Nat. Mater., 11 (**2012**) 963.

17. M. A. Lukowski, A. S. Daniel, F. Meng, A. Forticaux, L. Li, S. Jin, J. Am. Chem. Soc. 135 (**2013**) 10274.

18. T. F. Jaramillo, K. P. Jorgensen, J. Bonde, J. H. Nielsen, S. Horch, I. Chorkendorff, Science, 317 (**2007**) 100.

19. Z. Chen, D. Cummins, B. N. Reinecke, E. Clark, M. K. Sunkara, T. F. Jaramillo, Nano Lett. 11 (**2011**) 4168.

20. T. Wang, L. Liu, Z. Zhu, P. Papakonstantinou, J. Hu, H. Liu, M. Li, M. Energy Environ. Sci., 6 (**2013**) 625.

21. Y. Hou, A. B. Laursen, J. Zhang, G. Zhang, Y. Zhu, X. Wang, S. Dahl, I. Chorkendorff, Angew. Chem., Int. Ed., 52 (**2013**) 3621.

22. F. Meng, J. Li, S. K. Cushing, M. Zhi, N. Wu, J. Am. Chem. Soc., 135 (**2013**) 10286.

23. Y. H. Chang, C. T. Lin, T. Y. Chen, C. L. Hsu, Y. H. Lee, W. Zhang, K. H. Wei, L. J. Li, Adv. Mater., 25 (**2013**) 756.

24. J. D. Benck, Z. Chen, L. Y. Kuritzky, A. J. Forman, T. F. Jaramillo, ACS Catal., 2 (**2012**) 1916.

25. A. B. Laursen, P. C. K. Vesborg, I. Chorkendorff, Chem.Commun. 49 (**2013**) 4965.

26. B. Hinnemann, P. G. Moses, J. Bonde, K. P. Jorgensen, J. H. Nielsen, S. Horch, I. Chorkendorff, J. K. Norskov, J. Am. Chem. Soc., 127 (**2005**) 5308.

27. Y. Li, H. Wang, L. Xie, Y. Liang, G. Hong, H. Dai, J. Am. Chem. Soc., 133 (**2011**) 7296.

28. Y. Liang, Y. Li, H. Wang, H. Dai, J. Am. Chem. Soc., 135 (**2013**) 2013.

29. L. Liao, J. Zhu, X. Bian, L. Zhu, M. D. Scanlon, H. H. Girault, B. Liu, Adv. Fun. Mater., 23 (**2013**) 5326.

30. Z. S. Wu, S. Yang, Y. Sun, K. Parvez, X. Feng, K. Mullen, J. Am. Chem. Soc., 134 (**2012**) 9082.

31. Z. Y. Wang, H. Li, Z. Liu, Z. J. Shi, J. Lu, K. Suenaga, S. K. Joung, T. Okazaki, Z. N. Gu, J. Zhou, Z. X. Gao, G. P. Li, S. Sanvito, E. G. Wang, S. Iijima, J. Am. Chem.Soc., 132 (**2010**) 13840

32. K. Yan, L. Fu, H. L. Peng, Z. F. Liu, Acc. Chem. Res., 46 (**2013**) 2263.

33. Y. Hou , Z. Wen , S. Cui , X. Guo, J. Chen, Adv. Mater. 25 (**2013)** 6291.

34. D. Wang, Z. Wang, C. Wang, P. Zhou, Z. Wu, Z. Liu, Electrochem. Communi., 34 (**2013**) 219.

35. J. Xie, J. Zhang, S. Li, F. Grote, X. Zhang, H. Zhang, H. Zhang, R. Wang, Y. Lei, B. Pen, Y. Xie, J. Am. Chem. Soc., 135 (**2013**) 17881.

36. M. M. Titirici, M. Antonietti., Chem. Soc. Rev., 39 (**2010**) 103.

37. K. J. Huang, L. Wang, Y. J. Liu, T. Gan, Y. M. Liu, L. L. Wang, Y. Fan, Electrochim. Acta, 107 (**2013**) 379

38. N. Pentland, J. O. M. Bockris, E. Sheldon, J. Electrochem. Soc. 104 (**1957**) 182.

39. B. E. Conway, B. V. Tilak, Electrochim. Acta, 47 (**2002**) 3571.

40. Y. Yu, S. Y. Huang, Y. Li, S. N. Steinmann, W.Yang, L. Cao, Nano Lett., 14 (**2014**) 553.

41. J. Bonde, P. G. Moses, T. F. Jaramillo, J. K. Norskov, I. Chorkendorff, Faraday Discussions, 140 (**2008**) 219.

42. X. Bian, J. Zhu, L. Liao, M. D. Scanlon, P. Ge, C. Ji, H. H. Girault, B. Liu, Electrochem. Commun., 22 (**2012**) 128.

43. A. B. Laursen, S. Kegnas, S. Dahl, I. Chorkendorff, Energy and Environ. Sci.,5 (**2012**) 5577.

44. D. Kong, H. Wang, J. Cha, M. Pasta, K. Koski, J. Yao, Y. Cui, Nano Lett., 13 (**2013**) 1341.

Figure Captions

Figure 1: XRD patterns of the MoS_2 products obtained from various methods as indicated in the figure.

Figure 2: FE-SEM images of MoS_2 samples with **(A)** S01, nano-sheet morphology, **(B)** S02, nano-hollow-sphere morphology and **(C)** S03, nano-flake morphology respectively.

Figure 3: TEM images of MoS_2 samples with **(A, B)** S01, nano-sheet morphology, **(C, D)** S02, nano-hollow-sphere morphology and **(E, F)** S03, nano-flake morphology respectively.

Figure 4: (A) HAADF-STEM image of a selected nano-hollow-sphere of S02 sample, **(B)** corresponding EDS elemental depth profile measurement, **(C)** HAADF-STEM image of a selected nano-hollow-sphere and **(D, E)** corresponding EDS mapping images proves the structure is a hallow-bubble and both molybdenum, sulphur are enriched in the skin of the bubble.

Figure 5: Curve fitted XPS peaks for Mo atoms in various MoS_2 samples **(A)** S01; **(B)** S02 and **(C)** S03 prepared in this work.

Figure 6: Curve fitted XPS peaks for S atoms in various MoS_2 samples **(A)** S01; **(B)** S02 and **(C)** S03 prepared in this work.

Figure 7: (A) Polarization curves and **(B)** corresponding Tafel plots of various MoS_2 materials as shown in the figure.

Figure 8: Polarization curves revealing that negligible degradation of HER activity is observed for nano-hollow-sphere MoS_2 (S02) material even after 1000 CV cycles.

Table 1: A comparison of the exchange current density (j_0), Tafel slopes and onset potentials reported for various MoS_2 catalysts.

Catalyst	On-set potential (- mV/RHE)	j_0 ($A/cm^2_{geometric}$)	Tafel slope mV/decade	Reference
MoS_2 on Au(111)	--	3.1×10^{-7}	55-60	18
MoS_2	--	4.6×10^{-6}	120	41
MoS_2	--	--	53-65	24
MoS_2 on carbon nano-spheres	100	--	41	42
MoS_2/MWCNT	150-200	4.0×10^{-6}	109	43
MoS_2 on Au	90	9.3×10^{-6}	69	20
MoS_2	--	2.2×10^{-6}	105-120	44
MoS_2 grown on glassy carbon electrode	300	1.6×10^{-7}	142	40
MoS_2 Nano-sheets- S01	160	7.9×10^{-7}	124	This work

MoS_2 Nano-hollow-spheres- S02	110	5.0×10^{-6}	102	This work
MoS_2 Nano-flakes- S03	100	2.8×10^{-6}	148	This work

Hydrothermal assisted morphology designed MoS_2 material as alternative cathode catalyst for PEM electrolyser application

S. M. Senthil Kumar[*, A], *K. Selvakumar* [A], *R. Thangamuthu* [A], *A. Selvi* [B], *S. Ravichandran* [B], *G. Sozhan* [B], *K. Rajasekar* [C], *Nuria Navascues*[D], *Silvia Irusta* [D]

Figure 1

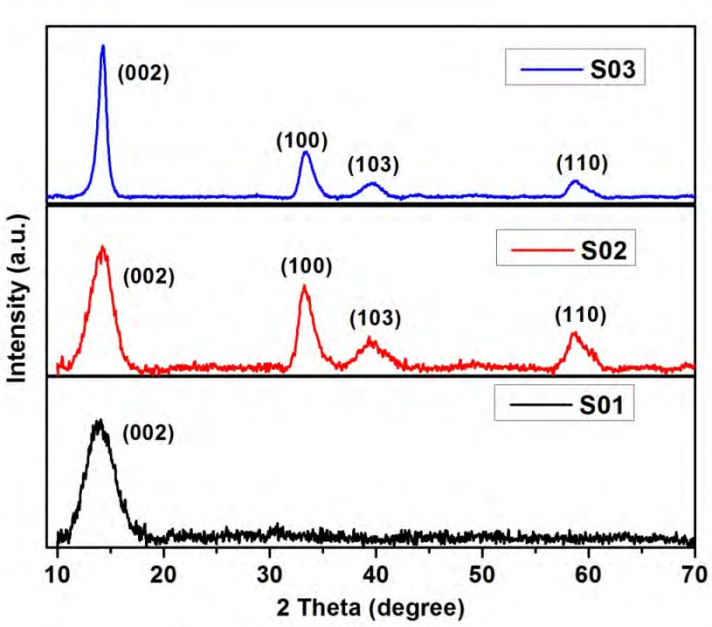

Figure 2

A

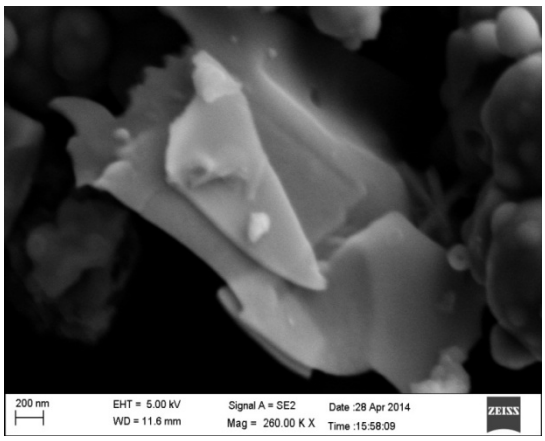
200 nm
EHT = 5.00 kV
WD = 11.6 mm
Signal A = SE2
Mag = 260.00 K X
Date :28 Apr 2014
Time :15:58:09
ZEISS

B

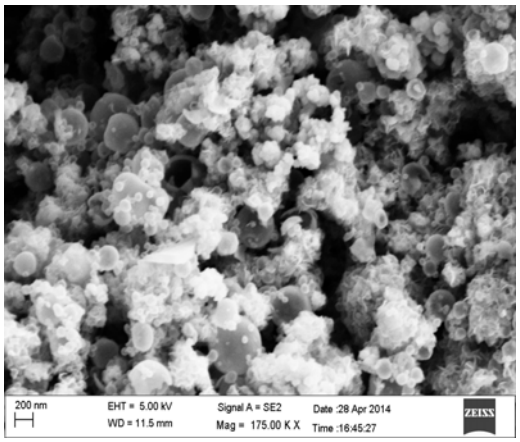
200 nm
EHT = 5.00 kV
WD = 11.5 mm
Signal A = SE2
Mag = 175.00 K X
Date :28 Apr 2014
Time :16:45:27
ZEISS

C

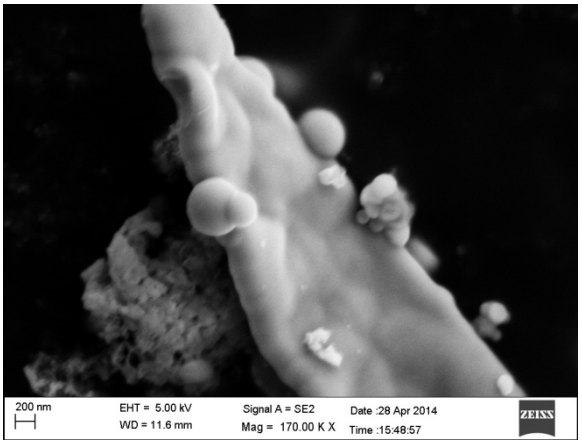
200 nm
EHT = 5.00 kV
WD = 11.6 mm
Signal A = SE2
Mag = 170.00 K X
Date :28 Apr 2014
Time :15:48:57
ZEISS

Figure 3

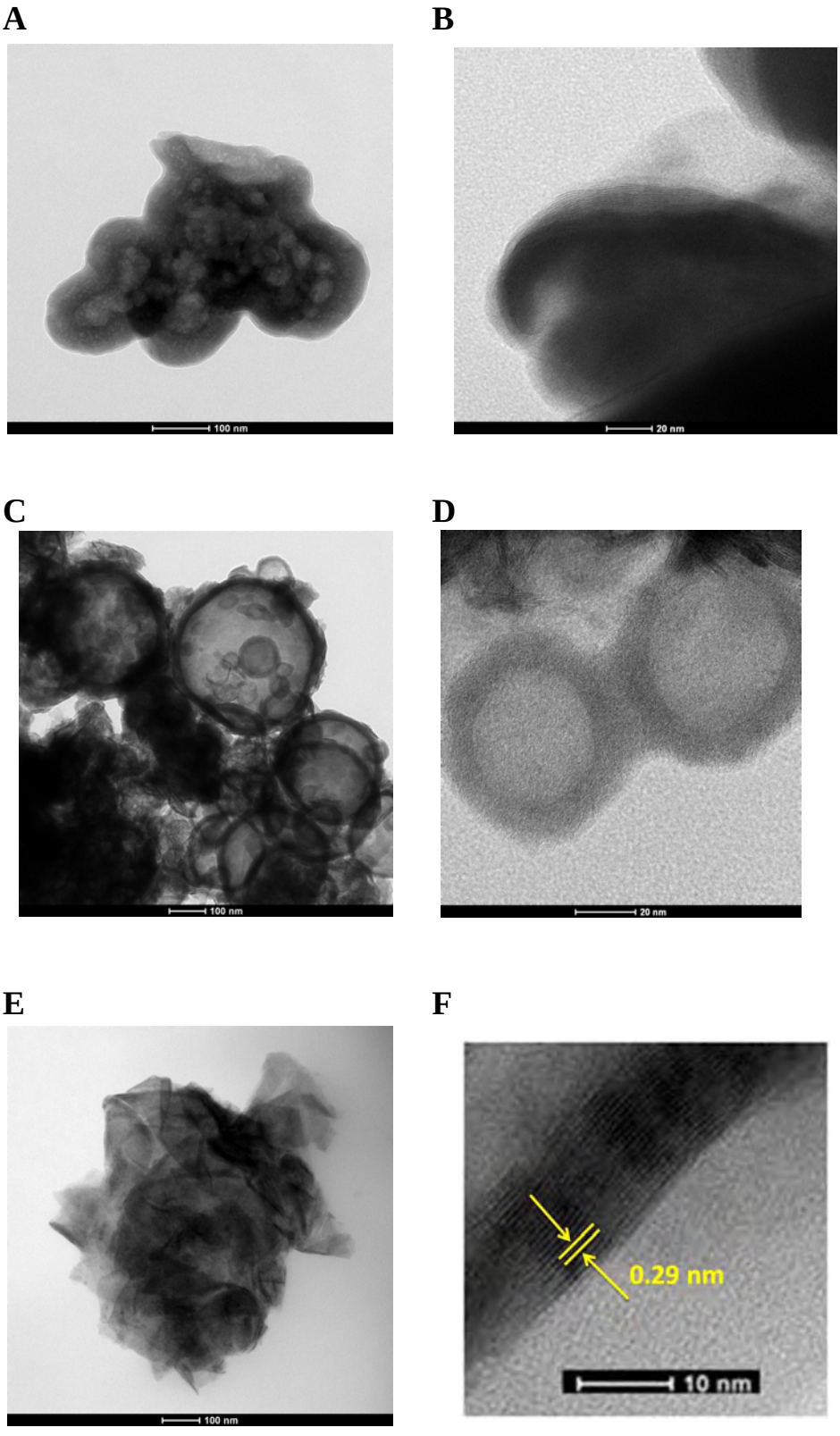

Figure 4

A

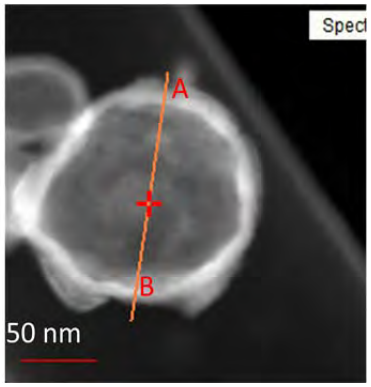

B

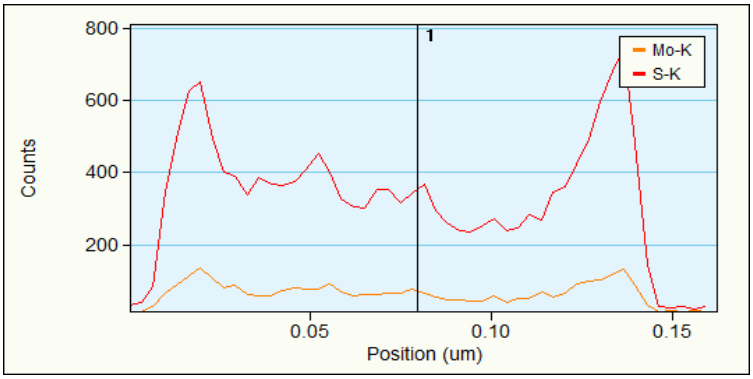

C

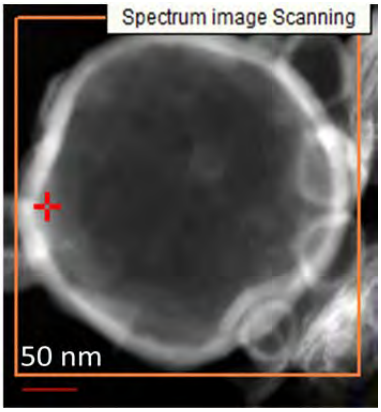

D

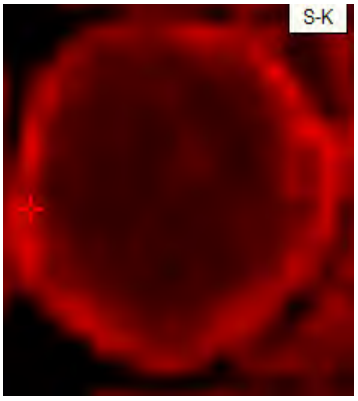

E

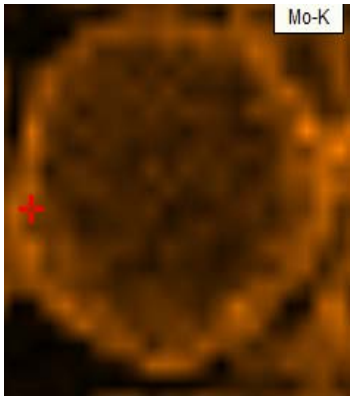

Figure 5

A

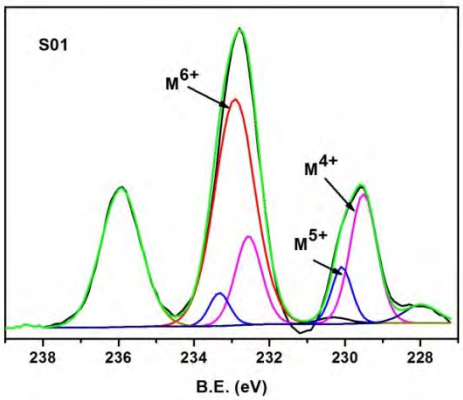
S01
M6+
M4+
M5+
238
236
234
232
230
228
B.E. (eV)

B

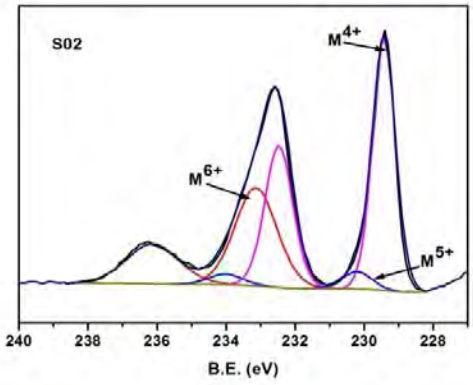
S02
M4+
M6+
M5+
240
238
236
234
232
230
228
B.E. (eV)

C

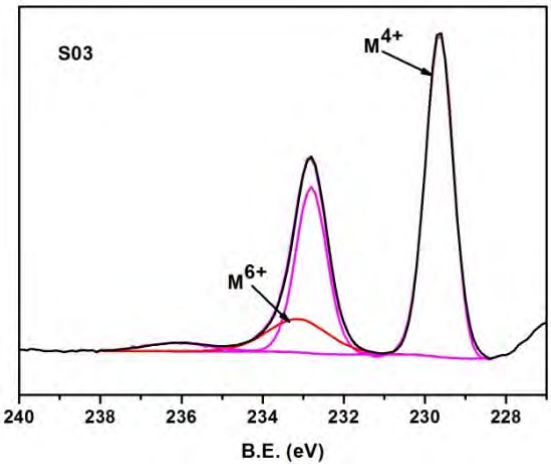
S03
M4+
M6+
240
238
236
234
232
230
228
B.E. (eV)

Figure 6

A

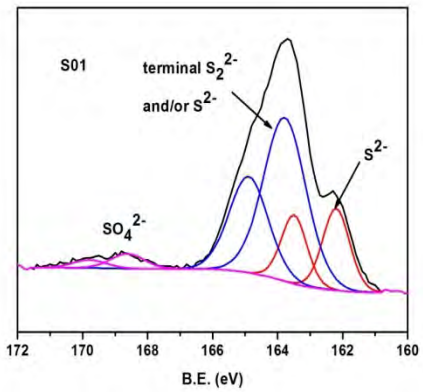
S01
terminal S_2^{2-}
and/or S^{2-}
S^{2-}
SO_4^{2-}
172
170
168
166
164
162
160
B.E. (eV)

B

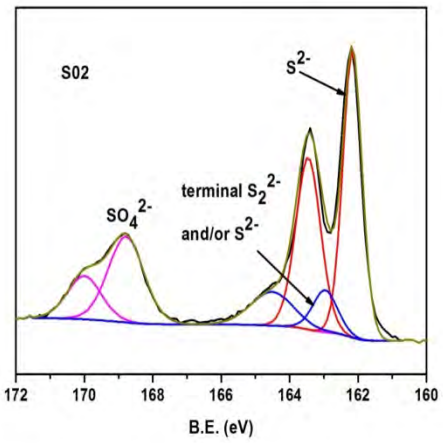
S02
S^{2-}
terminal S_2^{2-}
and/or S^{2-}
SO_4^{2-}
172
170
168
166
164
162
160
B.E. (eV)

C

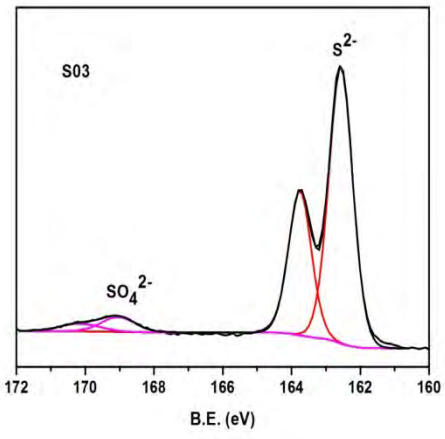
S03
S^{2-}
SO_4^{2-}
172
170
168
166
164
162
160
B.E. (eV)

Figure 7 **A**

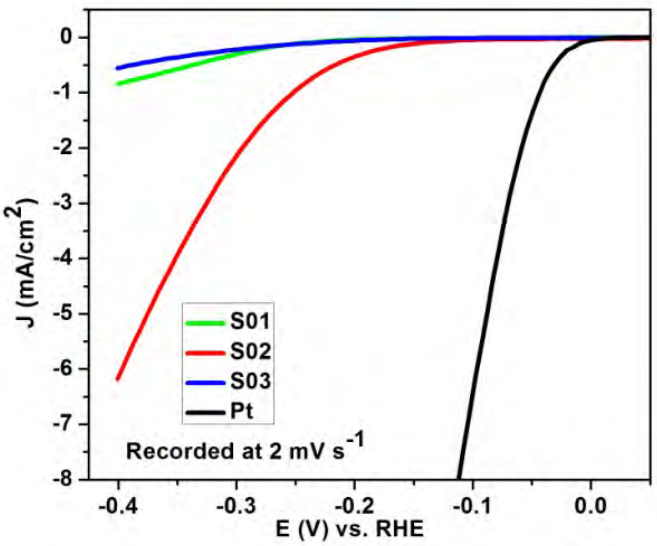
J (mA/cm^2)
E (V) vs. RHE
S01
S02
S03
Pt
Recorded at 2 mV s^{-1}

B

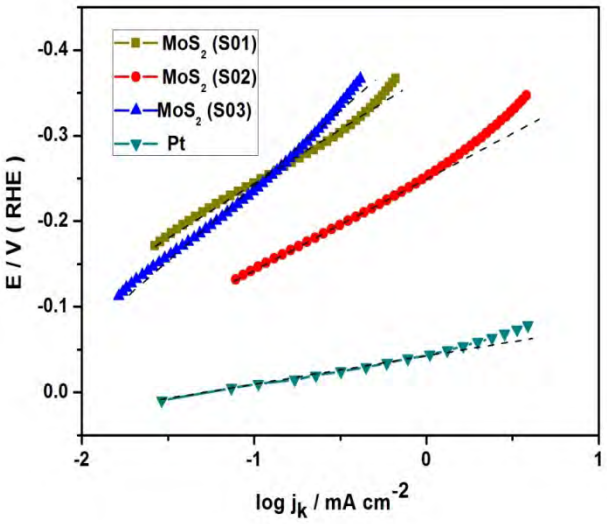
E / V (RHE)
log j_k / mA cm^{-2}
MoS$_2$ (S01)
MoS$_2$ (S02)
MoS$_2$ (S03)
Pt

Figure 8

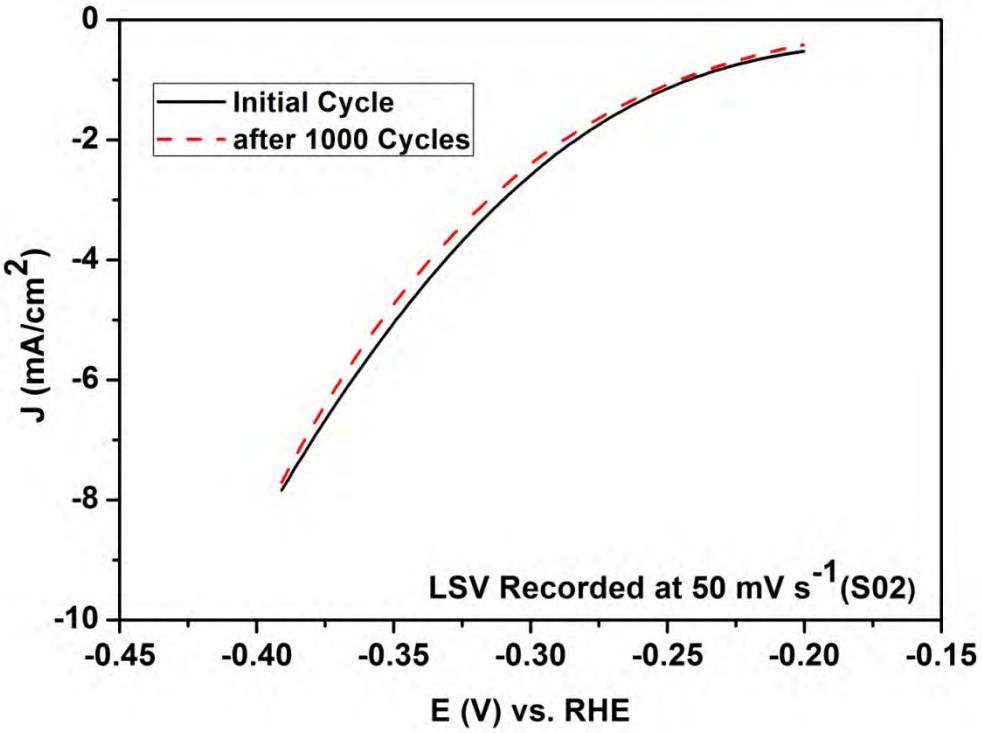
Initial Cycle
after 1000 Cycles
LSV Recorded at 50 mV s-1(S02)
J (mA/cm2)
E (V) vs. RHE
0
-2
-4
-6
-8
-10
-0.45
-0.40
-0.35
-0.30
-0.25
-0.20
-0.15